Original scientific paper

FIRST PRINCIPLE INSIGHT INTO Co-DOPED MoS2 FOR SENSING NH3 AND CH4 [*]

Bibek Chettri[1], Abinash Thapa[2], Sanat Kumar Das[1], Pronita Chettri[1], Bikash Sharma[2]

[1]Department of Physics, Sikkim Manipal Institute of Technology, Majitar, Sikkim, India
[2]Department of Electronics and Communication Engineering,
Sikkim Manipal Institute of Technology, Majitar, Sikkim, India

Abstract. *In this work we present the atomistic computational study of the adsorption properties of Co doped MoS_2 adsorbed ammonia (NH_3) and methane (CH_4). The adsorption distance, adsorption energy (E_{ad}), charge transfer (Q_t), bandgap, Density of States (DOS), Projected Density of States (PDOS), transport properties, sensitivity and recovery time have been reported. The diffusion property of the system was calculated using Nudge Elastic Band (NEB) method. The calculated results depict that after suitable doping of Co on MoS_2 monolayer decreases the resistivity of the system and makes it more suitable for application as a sensor. After adsorbing NH_3 and CH_4, Co doped MoS_2 bandgap, DOS and PDOS become more enhanced. The adsorption energy calculated for NH_3 and CH_4 adsorbed Co doped MoS_2 are -0.9 eV and -1.4 eV. The reaction is exothermic and spontaneous. The I-V curve for Co doped MoS_2 for CH_4 and NH_3 adsorption shows a linear increase in current up to 1.4 V and 2 V, respectively, then a rapid decline in current after increasing a few volts. The Co doped MoS_2 based sensor has a better relative resistance state, indicating that it can be employed as a sensor. The sensitivity for CH_4 and NH_3 were 124 % and 360.5 %, respectively, at 2 V. With a recovery time of 0.01s, the NH_3 system is the fastest. In a high-temperature condition/environment, the Co doped MoS_2 monolayer has the potential to adsorb NH_3 and CH_4 gas molecules. According to NEB, CH_4 gas molecules on Co doped MoS_2 has the lowest energy barrier as compared to NH_3 gas molecules. Our results indicate that adsorbing NH_3 and CH_4 molecules in the interlayer is an effective method for producing Co doped MoS_2 monolayers for use as spintronics sensor materials.*

Key words: *Density Functional Theory, gas sensor, adsorption energy, TMD.*

1. INTRODUCTION

NH_3 and CH_4 are the common gases which are used for industrial and agricultural purposes [1]. NH_3 and CH_4 are colourless and tasteless gases that are difficult to identify, and they make people suffocate when its concentration is high in the air [2][3][4]. CH_4 reduces the level of oxygen, resulting in headaches, dizziness, increased rate of heartbeat and causing breathlessness in human beings [5][6][7]. Therefore, good and sensitive gas sensors for the detection of hazardous gases such as ammonia (NH_3) and methane (CH_4), is critical for both industrial and civilian purposes [8][9][10]. Hence, the demand for gas sensors with high sensitivity, low power consumption and short recovery time has increased [11][12].

In recent years, two-dimensional (2D) materials such as Transition Metal Dichalcogenides (TMDs) have gained immense attention. 2D MoS_2, n-type semiconductor [13] with a bandgap of 1.3-1.8 eV [13][14][15] has been one of the most promising materials for the application of gas sensors due to its superior sensitivity [16][17]. MoS_2 monolayer has a large surface-to-volume ratio[18], tunable electrical properties [19][20] and magnetic properties [21][22]. Much research has been focused on making MoS_2 more prominent by suitable doping [23][24]. Xianxian et al. investigated the adsorption behaviour of Rh-doped MoS_2 monolayer towards SO_2, SOF_2 and SO_2F_2 and found the improved performance towards the adsorption of gas molecules as compared to pristine MoS_2 [25]. Guochao et al. verified the excellent sensitivity property of Au doped MoS_2 for sensing C_2H_6 and C_2H_2 [26]. Likewise, Zhen et al. confirmed the center of MoS_2 as the best possible site for doping Fe, Co, Ni and Cu [27]. The doping and codoping on MoS_2 confirmed the high sensitivity of NO and NO_2 gas by Ehab et al. [28]. Not only in MoS_2 but doping has significantly increased the material properties of other nanomaterials [29]. Chettri et al. explored the changes in the electronic and magnetic properties of *h*-BN after suitable doping [30].

Y. Wang et al. used DFT to determine that Fe doped MoS_2 could be used as a spintronic gas sensor to detect NO gas molecules [31]. Additionally, using DFT, Y.-H. Zhang et al. discovered that transition metal-doped MoS_2 can be used as a spintronic gas sensor to detect CO gas molecules [32]. The gas sensing properties of Pt_n doped WSe_2 nanosheet to SF_6 breakdown products were explored by Linga Xu et al., who discovered that incorporating a Pt atom greatly increases the sensing properties of WSe_2 nanosheet [33]. The overall results show the novelty of MoS_2 after suitable doping. Transition Metal (TM) doped MoS_2 are more prominent since the interaction between TM and MoS_2 is strong [1] and provides numerous free electrons [34][1]. Due to the strong orbital hybridization between the atoms and gas molecules, increased sensitivity is observed [35].

In this paper, we explored the adsorption properties of a Co doped monolayer (hereafter referred to as Co-MoS_2). The adsorption distance, binding energy, adsorption energy and charge transfer were studied to investigate the most stable configuration of doping of Co and adsorption of gas molecules on MoS_2 monolayer. Further, the bandgap, Density of States (DOS) and Projected Density of States (PDOS) were studied to understand the electronic properties. In the end, the I-V characteristics followed by sensitivity and recovery time was calculated to understand the property of the gas sensor.

2. Methodology

Density functional theory [36] computation was carried out in QuantumATK [37]. For the exchange-correlation term, the Perdew-Burke-Ernzerh Generalised Gradient Approximation (GGA-PBE) function was used [38][39] with Troullier-Martins type pseudopotential [40]. The non-conserving Double-Zeta Polarized (DZP) was used as the basis set [41] with a 5×5×1 Monkhorst-pack k-point grid [42]. The Density of States was computed with a higher k-point of 15×15×1 [32]. To understand the magnetic characteristics of the system, we used spin-polarized computations for all calculations [31]. The geometry was relaxed with limited memory Broyden-Fletcher-Goldfarb-Shanno (LBFGS) algorithm [43] with a minimum force of 0.05 eV/Å [43]. The considered cut-off energy for all the calculations was 100 Ha. The inclusion of dispersion correction is described by Grimme's DFT-D2 method. Pulay mixer algorithm was implemented to control the self-consistent iteration with a tolerance of 0.0002 Ry and 100 maximum steps [44]. The 4×4×1 supercell of MoS$_2$ monolayer with 15 Å vacuum space along z-direction was considered for the calculation with 32 S atoms and 16 Mo atoms. The calculated lattice constant of MoS$_2$ is 3.8 Å, which satisfies the theoretical value [45][46]. The MoS$_2$ monolayer was fully relaxed with Stillinger-Weber (SW) potentials [47].

The binding energy of Co-MoS$_2$ is calculated using [48],

$$E_b = E_{MoS_2} + E_{Co} - E_{Co-MoS_2}$$

Here, E_{MoS_2}, E_{Co} and E_{Co-MoS_2} represents the total energy of pristine MoS$_2$, isolated Co and Co-MoS$_2$ monolayer respectively.

The adsorption energy of NH$_3$ and CH$_4$ gas molecules on the Co-MoS$_2$ is calculated using[48],

$$E_{ads} = E_{Co-MoS_2} + E_{gas} - E_{Co-MoS_2-gas}$$

Here, E_{Co-MoS_2}, E_{gas} and E_{Co-MoS_2-gas} represents the total energy of Co-MoS$_2$ monolayer, isolated gas molecules and gas molecules adsorbed in Co-MoS$_2$ monolayer respectively.

The total charge transfer Q_t was obtained using the Mulliken method [49]. The Q_t is calculated by [49],

$$Q_t = Q_{absorbed(gas)} - Q_{isolated(gas)}$$

$Q_{absorbed(gas)}$ and $Q_{isolated(gas)}$ is the carried charge of gas molecules before and after gas adsorption respectively.

We used a two-probe configuration with the left electrode, right electrode, and central region to investigate the system's transport properties [50]. The Non Equilibrium Green's Function (NEGF) approach, as implemented in QuantumATK [51], was used to compute the transport properties of the considered structure. The device supercell was sampled using a 2 D Fast Fourier Transform (FFT2D) Poisson solver with 1×1×150 k-points for the device simulation [41]. On the electrode faces, the Dirichlet boundary condition is used, whereas, on all other faces, the boundary condition is set to periodic. For all device computations, the average Fermi level is used as the energy zero parameter in the Krylov self-energy calculator. The transmission is derived from the device's extended green's function as follows:

$$T(E) = Tr[\Gamma_L G^{\dagger} \Gamma_R G]$$

The greens' function is given by [52][53]

$$G(E) = [ES - H - \Sigma_L(E) - \Sigma_R(E)]^{-1}$$

The current voltage characteristics are now derived using the following equation by integrating the transmission function across a suitable voltage [54].

$$I(V_a) = G_0 \int_{E_f - ev_a/2}^{E_f + ev_a/2} T(E, V_a)dE$$

The sensitivity of the Co-MoS$_2$ to absorb urea and methanol was analyzed, obtained from the equation [55]

$$S = [(R - R_0)/R_0] \times 100\%$$

where R_0 and R represent the resistance of Co-MoS2 without and with gas adsorption respectively.

In addition, to study the property of gas sensors we estimated the recovery time. The better property of the gas sensor is predicted by a faster recovery time [50]. The recovery time is calculated using the following formula [56]:

$$\tau = A^{-1} e^{\frac{E_a}{k_B T}}$$

where A is the apparent factor which is equal to 10^{12} s^{-1}, k_B is the Boltzmann constant (8.62 $\times 10^{-5}$ eV/K. E_a is the absolute value of adsorption energy and T is the temperature [57].

The diffusion coefficient is calculated using the equation below [58][59].

$$D = \frac{1}{6N} \lim_{t \to \infty} \frac{d}{dt} \sum_{i=1}^{N} \langle [r_i(t) - r_0(t^2)] \rangle$$

Where $r_i(t)$ denotes the position of atom i at time of t, N is the number of diffusion atoms in the system, $r_0(t)$ is the initial position of atom i.

3. RESULT AND DISCUSSION

The structure of NH$_3$ and CH$_4$ is shown in Fig.1 (a) and (b) respectively. The central N atom in NH$_3$ molecules bonds with three H atoms. The bond length of N with three H atoms is 1 Å with a bond angle of 108.03°. The central C atom bonds with four H atoms in CH$_4$ molecules with bond length and bond angle of 1.09Å and 109.47° respectively. As per the Mulliken population analysis, the N and H atoms have a positive charge of 4.941e and 1.019e respectively in NH$_3$. The C and H atoms have the positive charge of 3.776e and 1.056e respectively in CH$_4$ molecules as calculated by the Mulliken population analysis. Table 1 summarizes the respective values.
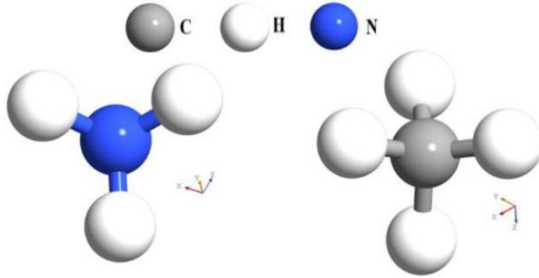
Fig. 1 The structure of (a) NH$_3$ and (b) CH$_4$

Table 1 Parameters for NH$_3$ and CH$_4$

Molecules	Bond Distance	Bond Angle	Q$_t$(e)
CH$_4$	C-H: 1.09Å	C-H: 109.47°	C: 3.776
			H: 1.056
NH$_3$	N-H: 1 Å	N-H: 108.03°	N: 4.941
			H: 1.019

The most stable structure of the Co-doped monolayer was obtained by calculating the binding energy, charge transfer and distance between the atoms for three positions where Co atom was kept on the top of S atom (S$_T$), top of Mo atom (Mo$_T$) and above the hexagonal ring (hollow) of MoS$_2$. The calculated parameters are shown in Table 1. The calculated binding energy for the hollow site is 3.97 eV and the total charge transfer is -0.003e. The distance between S and Mo atoms is 1.41 Å and 3.54 Å respectively. The binding energy of the Mo$_T$ site was calculated to be highest, i.e., 4.54 Å and the lowest was for the S$_T$ site i.e., -4.3 Å. The charge transfer of Mo$_T$ and S$_T$ is 0.021e and 0.163e. For the hollow site, the Co loses electrons on the hollow site after doping, whereas Co gets electrons in Mo$_T$ and S$_T$ site after doping. From here we can conclude that the Mo$_T$ site has strong binding energy and a shorter distance between S-Co and Mo-Co atoms. The binding is relatively strong, and Mo$_T$ is the most favorable position for the Co atom doped on the MoS$_2$ monolayer. The most stable structure Co on top of Mo atom (Mo$_T$) is shown in Fig. 2 (b) and (c).

(a) Top View

(b) Side View

(c) Top View
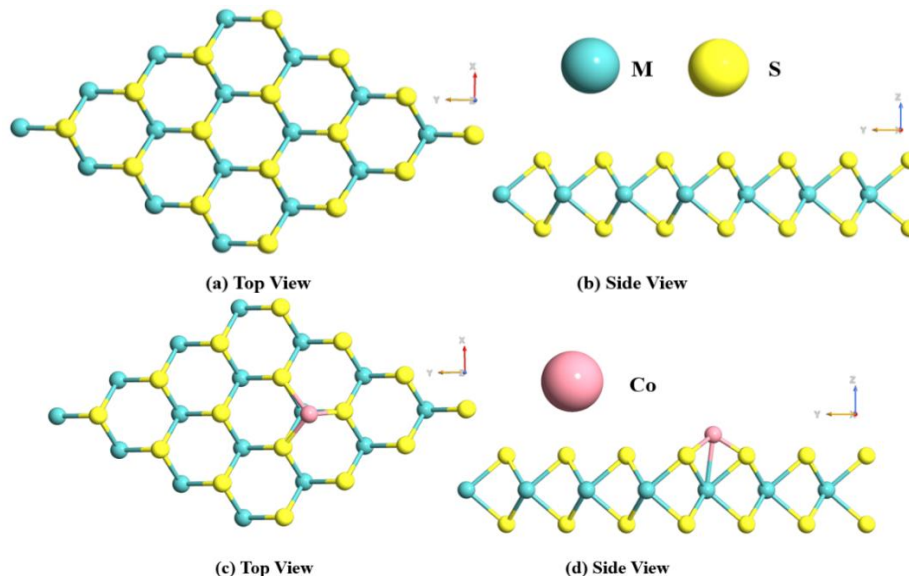
(d) Side View

Fig. 2 The structure of (a) top view, (b) side view of MoS$_2$, (c) top view and (d) side view of Co- MoS$_2$

Table 2 Parameters for Co-MoS$_2$

Site	E_b(eV)	Q_t(e)	d_s(Å)	d_{Mo}(Å)
S_T	-4.3	0.163	1.41	3.54
Mo_T	4.5	0.021	1.81	2.58
Hollow	3.9	-0.003	2.26	3.09

Furtheron, to investigate more about the effect of Co on MoS$_2$, we calculated the electronic properties like bandgap, the Density of States (DOS) and Projected Density of States (PDOS) of pristine MoS$_2$ monolayer and Co-MoS$_2$ monolayer. The optimized structure of the MoS$_2$ monolayer is shown in Fig. 2 (a) and (b). The bond length between Mo and S atom is 2.42 Å and the bond angle of S-Mo-S is 81.63°, which is close to the previous study [60]. The calculated band gap of pristine MoS$_2$ is 1.68 eV and after substitution of Co atom, bandgap reduces to 0.2 eV. The bandgap value calculated for monolayer MoS$_2$ is consistent with earlier literature [25][61][20]. The reduction in bandgap signifies the improvement in the conduction property of the material. It depicts the less energy required for the transition of electrons between the valence band and conduction band. The band structure of pristine MoS$_2$ and Co-MoS$_2$ is shown in Fig. 3 (a) and (b) respectively. The DOS graph of pristine MoS$_2$ is shown in Fig. 5 (a). The black and red lines in this diagram represent spin up and down, respectively. The DOS distance between the valence band and conduction band separation is much similar to the band structure of
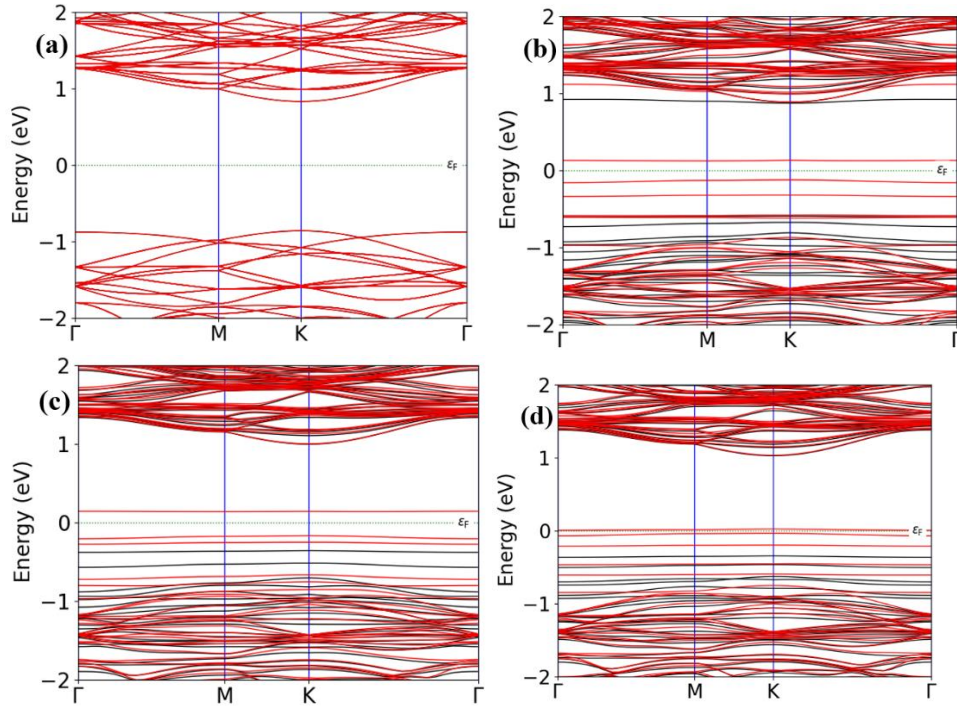
Fig. 3 The calculated Bandgap of (a) Pristine MoS$_2$, (b) Co-MoS$_2$, (c) Co-MoS$_2$ adsorbed CH$_4$ and (d) Co-MoS$_2$ adsorbed NH$_3$

pristine MoS$_2$. The DOS of pure MoS$_2$ is symmetric, with spin up and spin down mirroring each other. This result indicates that MoS$_2$ in its purest form is not magnetic. To better understand the electrical property, we looked at the PDOS of pristine MoS$_2$, as seen in Fig. 6(a). The p orbitals of S atoms dominate the upper and lower parts of the valence band. Similarly, Mo atoms d orbitals dominate the higher and lower parts of the conduction band. In both the upper and lower sides of the conduction band and valence band, there is a significant overlap of the p orbital of the S atom with the d orbital of the Mo atoms near the Fermi level. The strong hybridization of both atoms was shown by this overlap. Fig. 5 (b) and 6 (b) show the DOS and PDOS graphs for Co-MoS$_2$, respectively. The Co-d orbital contributes to the introduction of impurity states around the Fermi level, narrowing the energy bandgap to 0.2 eV. Because of the antisymmetric spin-up and spin-down states, the computed PDOS shows that the system has now become magnetic. The hybridization around the Fermi level of the conduction band is due to the d orbitals of Mo atoms and the d orbitals of Co atoms, according to the PDOS. Similarly, p orbitals of S atoms and d orbitals of Co atoms cause hybridization near the Fermi level of the valence band. Both the lower and upper sides of the conduction and valence bands show hybridization.

3.1. Adsorption Property of CH$_4$ and NH$_3$ on Co-MoS$_2$

To investigate the most stable position for the adsorption of CH$_4$ molecules on Co-MoS$_2$, we used three possible sites. Table 3 summarizes the adsorption energy, charge transfer, and adsorption distance calculations. The C atom was placed close to the Co atom (C-Co), the H atom was placed close to the Co atom (H-Co), and both the H and C atoms were placed close to the Co atom (H-C-Co). The adsorption energy for H-Co was calculated to be -0.2 eV, and the distance between H-Co was calculated to be 1.37. The adsorption energy for C-Co was determined to be 0.1 eV. For the H-C-Co position, higher adsorption energy of -1.4 eV was calculated. It adsorbs gas molecules at 1.75 for C-Co atoms and 1.57 for H-Co atoms. Because of the position of CH$_4$ that was kept above Co-MoS$_2$, there is a slight increase in adsorption distance when compared to the other two positions. Furthermore, the charge transfer for all three positions was calculated using Mulliken analysis. The total charge transfer Q_t was negative for all three positions, indicating that CH$_4$ molecules act as an electron donor, transferring an electron to Co-MoS$_2$. C-Co, H-Co, and H-C-Co locations have Q_t values of -0.116e, -0.17e, and -0.076e, respectively. As a result of the aforesaid results, we determined that the H-C-Co site is the most stable for CH$_4$ molecule adsorption on a Co-MoS$_2$ monolayer. Furthermore, we investigated the H-C-Co site adsorption ability for CH$_4$ molecule adsorption on Co-MoS$_2$. Fig. 4 (c) and 4 (d) depicts the most stable position. At energies of -0.17 eV, -0.18 eV, -0.19 eV, -0.2 eV, and -0.3 eV, a strong peak in the valence band, which is more populated than the conduction band, can be seen. In order to better understand the role of spin density at the Fermi level, we show the PDOS of CH$_4$ in Co-MoS$_2$ in Fig. 6. (c). The s, p, and d orbitals of the H, C, and Co, atoms have high peaks around the Fermi level of the upper and lower valence band, respectively. At the lower side of the conduction band, substantial hybridization of the s, p, and d orbitals of H, C, and Co atoms can be seen, indicating a large contribution to spin polarization from the CH$_4$ molecule. Our findings imply that adsorbing CH$_4$ molecules in the interlayer is a good way to create a Co-MoS$_2$ monolayer as a spintronics sensor material. When MoS$_2$ is doped with Co, it becomes a spintronics-based CH$_4$ sensor.

(a) Top View   **(b) Side View**

(c) Top View   **(d) Side View**
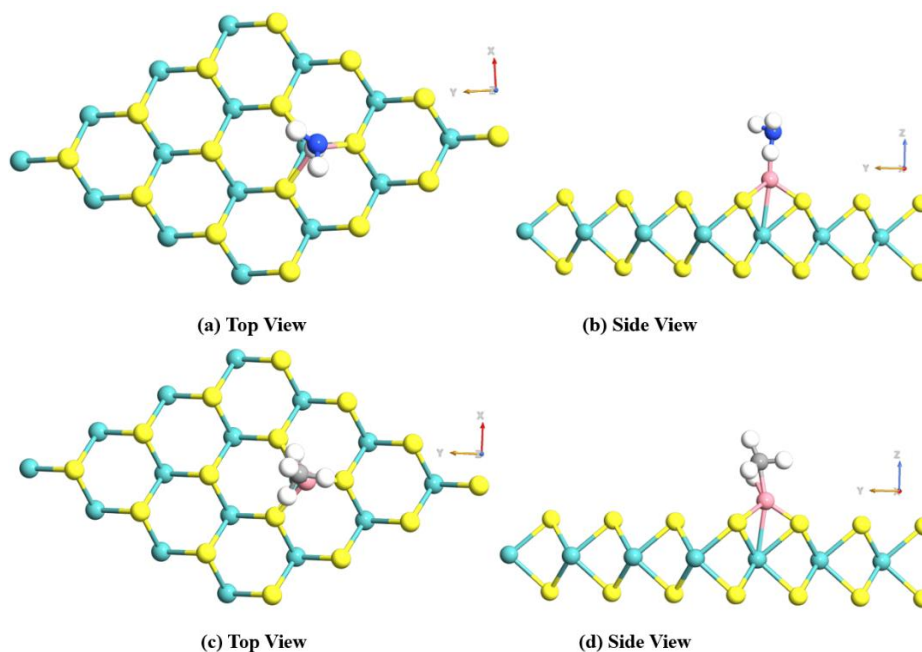
Fig. 4 The structure of (a) top view, (b) side view of adsorbed NH_3, (c) top view and (d) side view of adsorbed CH_4 in Co-MoS_2

Table 3 Parameters for adsorption of NH_3 on Co-MoS_2

Site	E_{ad}(eV)	Q_t(e)	distance(Å)
H-Co	-0.9	-0.173	H-Co: 1.23
N-Co	-0.8	-0.436	N-Co: 1.28
H-N-Co	-0.1	-0.114	H-Co: 1.55; N-Co: 1.89

Table 4 Parameters for adsorption of CH_4 on Co-MoS_2

Site	E_{ad}(eV)	Q_t(e)	distance(Å)
C-Co	0.1	-0.116	C-Co: 1.95
H-Co	-0.2	-0.17	H-Co: 1.37
H-C-Co	-1.4	-0.076	C-Co: 1.75; H-Co: 1.57
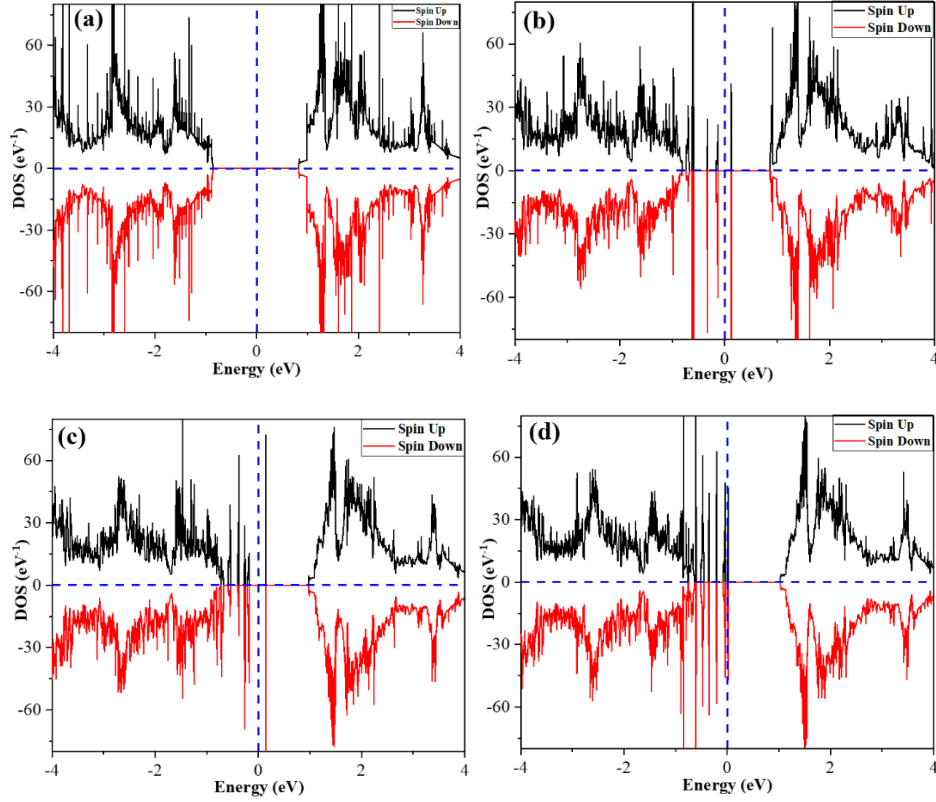
Fig. 5 Density of States of (a) Pristine MoS$_2$, (b) Co-MoS2, (c) adsorbed NH$_3$ and (d) adsorbed CH$_4$ on Co-MoS$_2$

We adopted three types of models to investigate the most stable site for the adsorption of NH$_3$ molecules on a Co-MoS$_2$ monolayer. The H atom was placed near the Co atom (H-Co), the N atom was placed near the Co atom (N-Co) and N and H atoms were placed near the Co atom (H-N-Co). The calculated parameters of the aforesaid site are presented in Table 3. The lowest adsorption energy was calculated for the H-No-Co site of -0.1 eV followed by the N-Co site of -0.8 eV. The highest adsorption energy was obtained for the H-Co site of -0.9 eV. When adsorption energy is negative, the adsorption process is exothermic. The adsorption distance of the H-N-Co site is 1.55 Å for H-Co and 1.89 Å for the N-Co bond, respectively. There was observed some reduction in adsorption distance of N-Co i.e., 1.28 Å. This might be affected by the alignment of NH$_3$ molecules kept near Co-MoS$_2$. For the H-Co site, the adsorption distance was reduced to 1.23 Å indicating the shortest adsorption distance among all the sites. The shorter adsorption distance signifies the adsorption between gas molecules and the Co-MoS$_2$ monolayer has a strong interaction. In addition, the total charge transfer Q$_t$ obtained by Mulliken analysis was found to be negative for all the sites. The negative Q$_t$ indicates that NH$_3$ acts as an electron donor and transfers an electron to Co-MoS$_2$. The corresponding total charge transfer of H-Co, N-Co and H-N-Co sites are -0.173e, -0.436e and -0.114e respectively. Due to the shorter adsorption distance, strong adsorption energy and

negative Q_t, the H-Co site is considered as one of the most stable sites for adsorption of NH_3 on Co-MoS_2. Furthermore, we calculated the bandgap, DOS and PDOS to understand the electronic property of the H-Co side. The most stable site is shown in Fig. 4 (a) and (b). The DOS for Co-MoS_2 adsorbed NH_3 is shown in Fig. 5 (d). In contrast to the cases where NH_3 was not adsorbed with Co-MoS_2, we discovered that when NH_3 is adsorbed with Co-MoS_2, a few new states near the Fermi level appear. Furthermore, the magnetic metal property with the spin channel in crossing the Fermi level with a bandgap of 0 eV is shown by the spin up and spin down. These conditions could be caused by the presence of the NH_3 molecule. The PDOS graph in Fig. 6 (d) shows the effects of NH_3 gas adsorption on Co-MoS_2. The primary peaks of NH_3 in Co-MoS_2 are formed by p orbitals of N atoms and are positioned at -0.3 eV and 0 eV, as seen in Fig. 6 (d). H atoms orbitals produce states with energies of 4.9 eV, which is far from the Fermi level. Although the contributions of the p orbitals are close to the Fermi level, their peaks are much weaker than those of the s orbitals. The d orbitals of Co atoms also produce some impurities around the bottom side of the Fermi level. As seen in PDOS, the d and p orbitals of the Co and N atoms play a key role in enhancing the conductivity of the NH_3 adsorbed system. Our findings suggest that adsorbing NH_3 molecules in the interlayer is a promising technique to make a Co-MoS_2 monolayer that can be used as a spintronics sensor. MoS_2 becomes a spintronics-based NH_3 sensor when it is doped with Co.
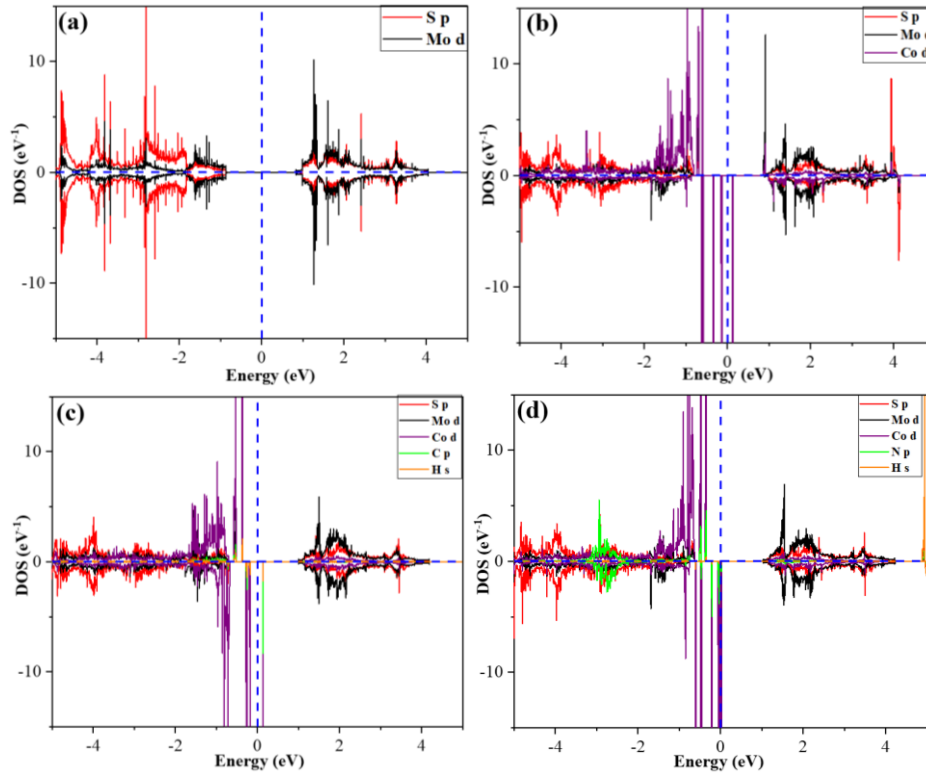
Fig. 6 Projected Density of States of (a) Pristine MoS_2, (b) Co-MoS_2, (c) adsorbed NH_3 and (d) adsorbed CH_4 on Co-MoS_2

3.2. Transport Property of CH$_4$ and NH$_3$ on Co-MoS$_2$

The I-V characteristic curve aids in determining the sensing device resistance status. Fig.7 (a) and 7 (b) show the device supercells that we used in our calculations (b). Fig. 8 depicts the Co-MoS$_2$ sensor I-V characteristic curve. Currents in Co-MoS$_2$ increase linearly up to 5.8 µA when a bias voltage of 1.4 V is applied. There is a linear degradation in the current as the bias voltage is increased further. Similarly, the current value increases linearly with the bias voltage in the CH$_4$ and NH$_3$ configurations. The greatest current value, 9.2 µA, is achieved in the NH$_3$ configuration with a bias voltage of 2 V, as seen in the graph. In addition, with a 1.4 V applied bias voltage, a value of 5.8 µA is achieved in the CH$_4$ configuration. After that, it starts to decrease for both configurations and approaches the present minimum value. Table 5 shows the Co-MoS$_2$ based sensor resistance condition at 2 V. Table 5 shows that the Co-MoS$_2$ without the detecting gas has a high resistance state of 921 Ωk at 2 V. The variance of resistance in the NH$_3$ and CH$_4$ configurations at 2 V, i.e., 411 Ωk and 200 Ωk, is lower.
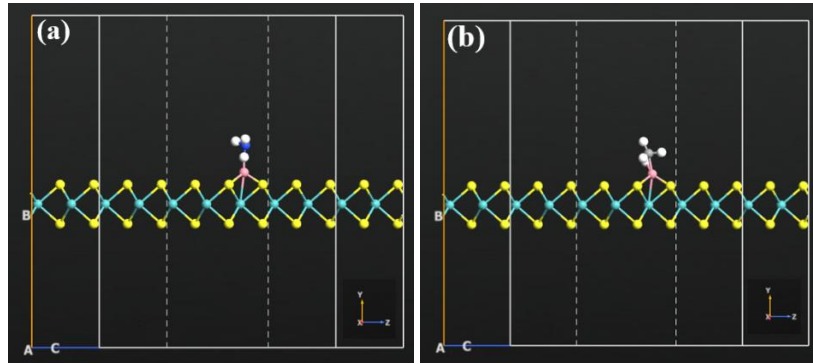
Fig. 7 Device Supercell of (a) NH$_3$ and (b) CH$_4$ on Co-MoS$_2$
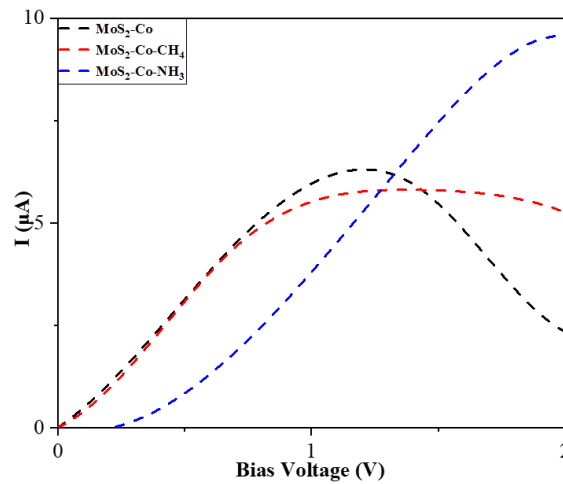
Fig. 8 I-V plot for Co-MoS$_2$ monolayer for adsorption NH$_3$ and CH$_4$

Table 5 The Co-MoS$_2$ based sensor resistance state at 2V

Device	Voltage (V)	Resistance (kΩ)
Co-MoS$_2$	2	921
Co-MoS$_2$-CH$_4$	2	411
Co-MoS$_2$-NH$_3$	2	200

3.3. Sensitivity, Recovery Time and Diffusion Barrier of CH$_4$ and NH$_3$ on Co-MoS$_2$

It is a well-known fact that a good sensor must have excellent selectivity to detect specific gas molecules. We also computed the sensitivity of CH$_4$ and NH$_3$ configurations for this purpose. To acquire a better understanding of the Co-MoS$_2$ monolayer sensitivity to targeted molecules at 2 V, we investigated it. The CH$_4$ adsorption sensitivity of Co-MoS$_2$ was 124 %. The sensitivity of Co-MoS$_2$ to NH$_3$ adsorption has also been calculated to be 360.5 %.

Table 6 Bandgap, sensitivity, and recovery time of CH$_4$ and NH$_3$ on Co-MoS$_2$

Configuration	Bandgap	Sensitivity	Recovery Time
Co-MoS$_2$-CH$_4$	-0.9	124%	1.4×10^8 s at 350 K
			4.7×10^5 s at 400k
			4.7×10^3 s at 450 K
Co-MoS$_2$-NH$_3$	-0.8	360.5%	9 s at 350 K
			0.2 s at 400k
			0.1 s at 450 K

Aside from that, the recovery time of methanol and urea on Co-MoS$_2$ is examined because reusability is an important indicator for gas sensors. The desorption time for the NH$_3$ arrangement is 9 s at 350 K and 0.2 sec at 400 K. At 450 K, the fastest recovery time was calculated to be 0.01 s for NH$_3$ molecules. At 450 K, the fastest recovery time for CH$_4$ molecules is 4.7×10^3 sec. At 400 K and 350 K, the recovery times were 4.3×10^5 sec and 1.4×10^8 sec, respectively. Because the CH$_4$ system has the maximum adsorption energy, the recovery rate is low. According to the computed value of recovery time, as the temperature rises, the recovery time decreases. Hence, NH$_3$ and CH$_4$ gas molecules adsorbed Co-MoS$_2$ monolayer is highly suitable for the application to monitor such gases in the furnace of industry.

The gas molecules diffusion characteristics in CH$_4$ and NH$_3$ on Co-MoS$_2$ are crucial for evaluating response performance, a quick diffusion of gas molecules in sensing material will result in a fast response and short recovery time of the gas sensor. As a result, the energy barriers of gases are calculated using the nudged elastic band (NEB) method in QuantumATK.

The gas molecules diffusion characteristics in Co-MoS$_2$ are crucial for evaluating response performance, a quick diffusion of gas molecules in sensing material will result in a fast response and short recovery time of the gas sensor [62][63][64]. As a result, the energy barriers of gases are calculated using the nudged elastic band (NEB) method in QuantumATK. For each of the nine diffusion images, the energy barrier of CH$_4$ and NH$_3$ gas molecules on Co-MoS$_2$ is computed. The initial path in our NEB calculation is image 1, and the final path is image 9. The image dependent pair potential approach with a

maximum distance of 1 Å was employed to develop the NEB image. The energy barrier for all the images is listed in Table 7. The diffusion barriers for CH$_4$ throughout the pathways vary from 0.01 eV to 1.69 eV, which is much lower than the NH$_3$ barrier ranges. The diffusion barrier for NH$_3$ varies from 0.89 eV to 5.15 eV along the paths. It means that CH$_4$ gas molecules diffuse considerably more easily than NH$_3$ gas molecules in Co-MoS$_2$. Furthermore, the diffusions of all gases in the Co-MoS$_2$ monolayer are not isotropic, image 1 to 9 for CH$_4$ gas molecules and image 1 to 2 for NH$_3$ gas molecules correspond to the lowest diffusion barrier, which is due to the inherent lack of electronic and structural symmetry [65].

Table 7 Diffusion barrier of CH$_4$ and NH$_3$ on Co-MoS$_2$

Diffusion Image	Diffusion Barriers (eV)	
	CH$_4$	NH$_3$
1 to 2	0.44	0.89
1 to 3	1.05	2.05
1 to 4	1.15	2.68
1 to 5	1.69	2.57
1 to 6	1.47	1.89
1 to 7	0.9	0.96
1 to 8	0.2	0.99
1 to 9	0.01	5.15
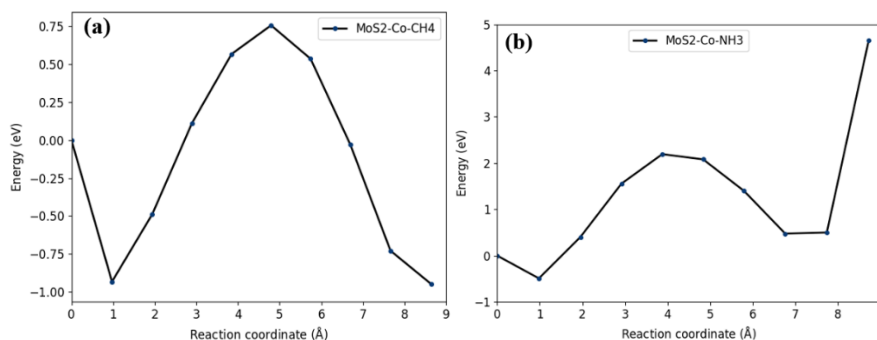
Fig. 9 Diffusion barrier of (a) CH$_4$ and (b) NH$_3$ on Co-MoS$_2$

4. CONCLUSION

Using the DFT method we investigated the adsorption distance, adsorption energy, charge transfer, bandgap, DOS, PDOS, transport property, sensitivity and recovery time of the NH$_3$ and CH$_4$ adsorbed Co-MoS$_2$ monolayer. The top of the Mo atom was calculated to be the stable position for the doping of the Co atom in MoS$_2$. The top of the Mo atom site has the highest binding energy of 4.5 eV. The doping of the Co atom in MoS$_2$ drastically reduces the bandgap to 1.19 eV from 1.68 eV. This suggests the conduction property of MoS$_2$ is enhanced. We found that NH$_3$ and CH$_4$ system has the shorter

adsorption distance. The adsorption energy of NH_3 and CH_4 systems are -0.9 eV and -1.4 eV. From the charge transfer, NH_3 and CH_4 molecules act as electron donors and Co-MoS_2 as an electron acceptor. After the Co atom was substituted in the MoS_2 monolayer, the magnetic property was detected. Our device has a linear increase in the current until 1.4 V and 2 V for CH_4 and NH_3 configurations, respectively, and shows variation in resistance, according to the I-V characteristics computed by NEGF. Furthermore, the Co-MoS_2 monolayer shows exceptional sensitivity for adsorbing CH_4 and NH_3 molecules, with the sensitivity of 124 % and 360.5 %, respectively. The recovery time suggests that NH_3 and CH_4 systems are suitable for high-temperature applications. The fastest recovery time was obtained for NH_3 with 0.01 s. According to the computed energy barrier, CH_4 gas molecules diffuse more easily in Co-MoS_2. Therefore, the Co-MoS_2 monolayer is suitable for the adsorption of NH_3 and CH_4 gas molecules and holds a high application in industrial purposes. As a result, the Co-MoS_2 monolayer appears to be a potential candidate for use as a spintronic sensor to detect NH_3 and CH_4 molecules.

REFERENCES

[1] P. Karki, B. Chettri, A. Thapa, P. Chettri and B. Sharma, "First Principle Study of MoS_2 adsorbed Transition Metal for Sensing NH_3 and CH^4", In Proceedings of the Devices for Integrated Circuit (DevIC), 2021, pp. 659–661.

[2] K. Wetchakun, T. Samerjai, N. Tamaekong, C. Liewhiran, C. Siriwong, V. Kruefu, A. Wisitsoraat, A. Tuantranont and S. Phanichphant, "Semiconducting metal oxides as sensors for environmentally hazardous gases", *Sens. Actuators B: Chem.*, vol. 160, no. 1, pp. 580–591, Dec. 2011.

[3] B. Tian, T. Huang, J. Guo, H. Shu, Y. Wang and J. Dai, "Gas adsorption on the pristine monolayer GeP_3 : A first-principles calculation", *Vacuum*, vol. 164, pp. 181–185, June 2019.

[4] R. Cao, B. Zhou, C. Jia, X. Zhang and Z. Jiang, "Theoretical study of the NO, NO_2, CO, SO_2, and NH_3 adsorptions on multi-diameter single-wall MoS_2 nanotube", *J. Phys. D. Appl. Phys.*, vol. 49, no. 4, p. 045106, Dec. 2015.

[5] T. Abbasi and S.A. Abbasi, ""Renewable" hydrogen: Prospects and challenges", *Renew. Sustain. Energy Rev.*, vol. 15, no. 6, pp. 3034–3040, Aug. 2011.

[6] F. Barbir, "Fuel cells and hydrogen economy", *Chem. Ind. Chem. Eng. Q.*, vol. 11, no. 3, pp. 105–113, June 2005.

[7] X. Cheng, Z. Shi, N. Glass, L. Zhang, J. Zhang, D. Song, Z. S. Liu, H. Wang and J. Shen, "A review of PEM hydrogen fuel cell contamination: Impacts, mechanisms, and mitigation", *J. Power Sources*, vol. 165, no. 2, pp. 739–756, Mar. 2007.

[8] H. Luo, Y. Cao, J. Zhou, J. Feng, J. Cao and H. Guo, "Adsorption of NO_2, NH_3 on monolayer MoS_2 doped with Al, Si, and P: A first-principles study", *Chem. Phys. Lett.*, vol. 643, pp. 27–33, Jan. 2016.

[9] D. J. Late, T. Doneux and M. Bougouma, "Single-layer $MoSe_2$ based NH_3 gas sensor", *Appl. Phys. Lett.*, vol. 105, p. 233103, Dec. 2014.

[10] N. Yamazoe, "Toward innovations of gas sensor technology", *Sensors Actuators, B Chem.*, vol. 108, pp. 2–14, July 2005.

[11] A. Zettl, "Extreme oxygen sensitivity of electronic properties of carbon nanotubes", *Science*, vol. 287, no. 5459, pp. 1801–1804, Mar. 2000.

[12] K. Kalantar-Zadeh and B. Fry, *Nanotechnology-enabled sensors*, Springer, 2008.

[13] Z. Huang, X. Peng, H. Yang, C. He, L. Xue, G. Hao, C. Zhang, W. Liu, X. Qi and J. Zhong, "The structural, electronic and magnetic properties of bi-layered MoS_2 with transition-metals doped in the interlayer", *RSC Adv.*, vol. 3, pp. 12939–12944, June 2013.

[14] Y. Zhang, W. Zeng and Y. Li, "The hydrothermal synthesis of 3D hierarchical porous MoS₂ microspheres assembled by nanosheets with excellent gas sensing properties", *J. Alloys Compd.*, vol. 749, pp. 355–362, June 2018.

[15] R. Wang, B. A. Ruzicka, N. Kumar, M. Z. Bellus, H.Y. Chiu and H. Zhao, "Ultrafast and spatially resolved studies of charge carriers in atomically thin molybdenum disulfide", *Phys. Rev. B - Condens. Matter Mater. Phys.*, vol. 86, p. 045406, July 2012.

[16] S. Cui, Z. Wen, X. Huang, J. Chang and J. Chen, "Stabilizing MoS2 nanosheets through SnO2 nanocrystal decoration for high-performance gas sensing in air", *Small*, vol. 11, no. 19, pp. 2305–2313, May 2015.

[17] Q. Zhou, C. Hong, Y. Yao, S. Hussain, L. Xu, Q. Zhang, Y. Gui and M. Wang, "Hierarchically MoS₂ nanospheres assembled from nanosheets for superior CO gas-sensing properties", *Mater. Res. Bull.*, vol. 101, pp. 132–139, May 2018.

[18] D. Zhang, J. Wu, P. Li and Y. Cao, "Room-temperature SO₂ gas-sensing properties based on a metal-doped MoS₂ nanoflower: An experimental and density functional theory investigation", *J. Mater. Chem. A*, vol. 5, pp. 20666–20677, Sep. 2017.

[19] D. J. Late, Y. K. Huang, B. Liu, J. Acharya, S. N. Shirodkar, J. Luo, A. Yan, D. Charles, U. V. Waghmare, V. P. Dravid and C. N. R. Rao, "Sensing behavior of atomically thin-layered MoS₂ transistors", *ACS Nano*, vol. 7, no. 6, pp. 4879–4891, May 2013.

[20] J. Wang, Q. Zhou, L. Xu, X. Gao and W. Zeng, "Gas sensing mechanism of dissolved gases in transformer oil on Ag–MoS₂ monolayer: A DFT study", *Phys. E Low-Dimensional Syst. Nanostructures*, vol. 118, p. 113947, Apr. 2020.

[21] A. M. Hu, L. L. Wang, W. Z. Xiao, G. Xiao and Q. Y. Rong, "Electronic structures and magnetic properties in nonmetallic element substituted MoS2 monolayer", *Comput. Mater. Sci.*, vol. 107, pp. 72–78, Sep. 2015.

[22] D. Ma, W. Ju, T. Li, X. Zhang, C. He, B. Ma, Y. Tang, Z. Lu and Z. Yang, "Modulating electronic, magnetic and chemical properties of MoS₂ monolayer sheets by substitutional doping with transition metals", *Appl. Surf. Sci.*, vol. 364, pp. 181–189, Feb. 2016.

[23] L. Zhang, T. Liu, T. Li and S. Hussain, "A study on monolayer MoS₂ doping at the S site via the first principle calculations", *Phys. E Low-Dimensional Syst. Nanostructures*, vol. 94, pp. 47–52, Oct. 2017.

[24] H. Cui, X. Zhang, G. Zhang and J. Tang, "Pd-doped MoS₂ monolayer: A promising candidate for DGA in transformer oil based on DFT method", *Appl. Surf. Sci.*, vol. 470, pp. 1035–1042, Mar. 2019.

[25] X. Gui, Q. Zhou, S. Peng, L. Xu and W. Zeng, "Adsorption behavior of Rh-doped MoS2 monolayer towards SO₂, SOF₂, SO₂F₂ based on DFT study", *Phys. E Low-Dimensional Syst. Nanostructures*, vol. 122, p. 114224, Aug. 2020.

[26] G. Qian, Q. Peng, D. Zou, S. Wang, B. Yan and Q. Zhou, "First-Principles Insight Into Au-Doped MoS₂ for Sensing C₂H₆ and C₂H₄," *Front. Mater.*, vol. 7, p. 22., Feb. 2020.

[27] Z. Xiao, W. Wu, X. Wu and Y. Zhang, "Adsorption of NO₂ on monolayer MoS₂ doped with Fe, Co, and Ni, Cu: A computational investigation", *Chem. Phys. Lett.*, vol. 755, p. 137768, Sep. 2020.

[28] E. Salih and A.I. Ayesh, "First principle study of transition metals codoped MoS₂ as a gas sensor for the detection of NO and NO₂ gases", *Phys. E Low-Dimensional Syst. Nanostructures*, vol. 131, p. 114736, July 2021.

[29] M. W. Iqbal, E. Elahi, A. Amin, G. Hussain and S. Aftab, "Chemical doping of transition metal dichalcogenides (TMDCs) based field effect transistors: A review", *Superlattices Microstruct.*, vol. 137, p. 106350, Jan. 2020.

[30] B. Chettri, P. K. Patra, Lalmuanchhana, Lalhriatzuala, S. Verma, B. K. Rao, M. L. Verma, V. Thakur, N. Kumar, N. N. Hieu and D.P. Rai, "Induced magnetic states upon electron–hole injection at B and N sites of hexagonal boron nitride bilayer: A density functional theory study", *Int. J. Quantum Chem.*, vol. 121, no. 16, p. e26680, Aug. 2021.

[31] Y. Wang, X. Shang, X. Wang, J. Tong and J. Xu, "Density functional theory calculations of NO molecule adsorption on monolayer MoS₂ doped by Fe atom", *Mod. Phys. Lett. B*, vol. 29, no. 27, p. 1550160, Oct. 2015.

[32] Y. H. Zhang, J. L. Chen, L. J. Yue, H. L. Zhang and F. Li, "Tuning CO sensing properties and magnetism of MoS₂ monolayer through anchoring transition metal dopants", *Comput. Theor. Chem.*, vol. 1104, pp. 12–17, Mar. 2017.

[33] L. Xu, Y. Gui, W. Li, Q. Li and X. Chen, "Gas-sensing properties of Ptn-doped WSe₂ to SF₆ decomposition products", *J. Ind. Eng. Chem.*, vol. 97, pp. 452–459, May 2021.

[34] P. Sharma, M. Lepcha, B. Chettri, A. Thapa, P. Chettri and B. Sharma, "First Principle Study of MoS₂ adsorbed Transition Metal for Sensing Urea and Methanol" , In Proceedings of the Devices for Integrated Circuit (DevIC), 2021, pp. 655–658.

[35] T. Li, Y. Gui, W. Zhao, C. Tang and X. Dong, "Palladium modified MoS$_2$ monolayer for adsorption and scavenging of SF6 decomposition products: A DFT study", *Phys. E Low-Dimensional Syst. Nanostructures*, vol. 123, p. 114178, Sep. 2020.

[36] S. Smidstrup, D. Stradi, J. Wellendorff, P. A. Khomyakov, U. G. Vej-Hansen, M.-E. Lee, T. Ghosh, E. Jónsson, H. Jónsson and K. Stokbro, "First-principles Green's-function method for surface calculations: A pseudopotential localized basis set approach", *Phys. Rev. B*, vol. 96, p. 195309, Nov. 2017.

[37] S. Smidstrup, T. Markussen, P. Vancraeyveld, J. Wellendorff, J. Schneider, T. Gunst, B. Verstichel, D. Stradi, P. A. Khomyakov, U. G. Vej-Hansen, others, "QuantumATK: An integrated platform of electronic and atomic-scale modelling tools", *J. Phys Condens. Matter.*, vol. 32, p. 15901, 2020.

[38] J. P. Perdew, K. Burke and M. Ernzerhof, "Generalized gradient approximation made simple", *Phys. Rev. Lett.*, vol. 77, p. 1396, Oct. 1996.

[39] J. P. Perdew, K. Burke and M. Ernzerhof, "Perdew, Burke, and Ernzerhof Reply", *Phys. Rev. Lett.*, vol. 80, p. 891, Jan. 1998.

[40] N. Troullier and J. L. Martins, "Efficient pseudopotentials for plane-wave calculations", *Phys. Rev. B*, vol. 43, no. 3, pp. 1993–2006, Jan. 1991.

[41] A. Sengupta, "On the junction physics of Schottky contact of (10, 10) MX$_2$ (MoS$_2$, WS$_2$) nanotube and (10, 10) carbon nanotube (CNT): an atomistic study", *Appl. Phys. A Mater. Sci. Process.*, vol. 123, p. 227, Mar. 2017.

[42] H. J. Monkhorst and J. D. Pack, "Special points for Brillouin-zone integrations", *Phys. Rev. B*, vol. 13, p. 5188, June 1976.

[43] J. Schneider, J. Hamaekers, S. T. Chill, S. Smidstrup, J. Bulin, R. Thesen, A. Blom and K. Stokbro, "ATK-ForceField: a new generation molecular dynamics software package", *Model. Simul. Mater. Sci. Eng.*, vol. 25, p. 85007, Oct. 2017.

[44] P. Pulay, "Convergence acceleration of iterative sequences. the case of scf iteration", *Chem. Phys. Lett.*, vol. 73, no. 2, pp. 393–398, July 1980.

[45] A. Ramasubramaniam and D. Naveh, "Mn-doped monolayer MoS$_2$: An atomically thin dilute magnetic semiconductor", *Phys. Rev. B - Condens. Matter Mater. Phys.*, vol. 87, p. 195201, May 2013.

[46] P. Wu, N. Yin, P. Li, W. Cheng and M. Huang, "The adsorption and diffusion behavior of noble metal adatoms (Pd, Pt, Cu, Ag and Au) on a MoS$_2$ monolayer: A first-principles study", *Phys. Chem. Chem. Phys.*, vol. 19, pp. 20713–20722, Aug. 2017.

[47] J. W. Jiang, H. S. Park and T. Rabczuk, "Molecular dynamics simulations of single-layer molybdenum disulphide (MoS$_2$): Stillinger-Weber parametrization, mechanical properties, and thermal conductivity", *J. Appl. Phys.*, vol. 114, p. 064307, Aug. 2013.

[48] Y. Li, X. Zhang, D. Chen, S. Xiao and J. Tang, "Adsorption behavior of COF$_2$ and CF$_4$ gas on the MoS$_2$ monolayer doped with Ni: A first-principles study", *Appl. Surf. Sci.*, vol. 443, pp. 274–279, June 2018.

[49] Y. Chen, X. Wang, C. Shi, L. Li, H. Qin and J. Hu, "Sensing mechanism of SnO2(1 1 0) surface to H$_2$: Density functional theory calculations", *Sensors Actuators, B Chem.*, vol. 220, pp. 279–287, Dec. 2015.

[50] D. Stradi, U. Martinez, A. Blom, M. Brandbyge and K. Stokbro, "General atomistic approach for modeling metal-semiconductor interfaces using density functional theory and nonequilibrium Green's function", *Phys. Rev. B*, vol. 93, p. 155302, Apr. 2016.

[51] M. Brandbyge, J.-L. Mozos, P. Ordejón, J. Taylor and K. Stokbro, "Density-functional method for nonequilibrium electron transport", *Phys. Rev. B*, vol. 65, p. 165401, Mar. 2002.

[52] S. Datta and H. van Houten, "Electronic Transport in Mesoscopic Systems", *Phys. Today*, vol. 49, no. 5, p. 70, May 1996.

[53] S. Datta, "Nanoscale device modeling: the Green's function method", *Superlattices Microstruct.*, vol. 28, no. 4, pp. 253–278, Oct. 2000.

[54] P. Srivastava, V. Sharma and N. K. Jaiswal, "Adsorption of COCl gas molecule on armchair boron nitride nanoribbons for nano sensor applications", *Microelectron. Eng.*, vol. 146, pp. 62–67, Oct. 2015.

[55] J. Prasongkit, V. Shukla, A. Grigoriev, R. Ahuja, V. Amornkitbamrung, "Ultrahigh-sensitive gas sensors based on doped phosphorene: A first-principles investigation", *Appl. Surf. Sci.*, vol. 497, p. 143660, Dec. 2019.

[56] Y. H. Zhang, Y. Bin Chen, K. G. Zhou, C. H. Liu, J. Zeng, H. L. Zhang and Y. Peng, "Improving gas sensing properties of graphene by introducing dopants and defects: A first-principles study", *Nanotechnol.*, vol. 20, no. 18, p. 185504, Apr. 2009.

[57] S. Peng, K. Cho, P. Qi and H. Dai, "Ab initio study of CNT NO$_2$ gas sensor", *Chem. Phys. Lett.*, vol. 387, pp. 271–276, Apr. 2004.

[58] G. Henkelman, B. P. Uberuaga and H. Jónsson, "Climbing image nudged elastic band method for finding saddle points and minimum energy paths", *J. Chem. Phys.*, vol. 113, p. 9901, Nov. 2000.

[59] G. Henkelman and H. Jónsson, "Improved tangent estimate in the nudged elastic band method for finding minimum energy paths and saddle points", *J. Chem. Phys.*, vol. 113, p. 9978, Nov. 2000.

[60] J. Wang, Q. Zhou, Z. Lu, Y. Gui and W. Zeng, "Adsorption of H$_2$O molecule on TM (Au, Ag)doped-MoS$_2$ monolayer: A first-principles study", *Phys. E Low-Dimensional Syst. Nanostructures*, vol. 113, pp. 72–78, Sep. 2019.

[61] S. Ahmad and S. Mukherjee, "A Comparative Study of Electronic Properties of Bulk MoS$_2$ and Its Monolayer Using DFT Technique: Application of Mechanical Strain on MoS$_2$ Monolayer", *Graphene*, vol. 3, no. 4, pp. 52–59, Oct. 2014.

[62] A. Ghosh and S. B. Majumder, "Modeling the sensing characteristics of chemi-resistive thin film semi-conducting gas sensors", *Phys. Chem. Chem. Phys.*, vol. 19, pp. 23431–23443, Sep. 2017.

[63] H. Wang, G. Gao, G. Wu, H. Zhao, W. Qi, K. Chen, W. Zhang and Y. Li, "Fast hydrogen diffusion induced by hydrogen pre-split for gasochromic based optical hydrogen sensors", *Int. J. Hydrogen Energy*, vol. 44, no. 29, pp. 15665–15676, June 2019.

[64] Y. Qiao, J. Wu, X. Cheng, Y. Pang, Z. Lu, X. Lou, Q. Li, J. Zhao, S. Yang and Y. Liu, "Construction of robust coupling interface between MoS$_2$ and nitrogen doped graphene for high performance sodium ion batteries", *J. Energy Chem.*, vol. 48, pp. 435–442, Sep. 2020.

[65] S. Mukherjee, A. Banwait, S. Grixti, N. Koratkar and C. V. Singh, "Adsorption and Diffusion of Lithium and Sodium on Defective Rhenium Disulfide: A First Principles Study", *ACS Appl. Mater. Interfaces*, vol. 10, no. 6, pp. 5373–5384, Jan. 2018.